INTERNATIONAL JOURNAL FOR NUMERICAL METHODS IN FLUIDS, VOL. 14, 1289–1310 (1992)

APPLICATION OF A VORTEX METHOD TO FREE SURFACE FLOWS

LIYONG CHEN

Alan C. McClure Associates, Inc., 2600 S. Gessner, Suite 504, Houston, TX 77063, U.S.A.

AND

WILLIAM S. VORUS

Department of Naval Architecture and Marine Engineering, University of Michigan, Ann Arbor, MI 48109-2145, U.S.A.

SUMMARY

Vortex methods have found wide applications in various practical problems. The use of vortex methods in free surface flow problems, however, is still very limited. This paper demonstrates a vortex method for practical computation of non-linear free surface flows produced by moving bodies. The method is a potential flow formulation which uses the exact non-linear free surface boundary condition at the exact location of the instantaneous free surface. The position of the free surface, on which vortices are distributed, is updated using a Lagrangian scheme following the fluid particles on the free surface. The vortex densities are updated by the non-linear dynamic boundary condition, derived from the Euler equations, with an iterative Lagrangian numerical scheme.

The formulation is tested numerically for a submerged circular cylinder in unsteady translation. The iteration is shown to converge for all cases. The results of the unsteady simulations agree well with classical linearized solutions. The stability of the method is also discussed.

KEY WORDS Vortex method Free surface flows Body–wave interaction

1. INTRODUCTION

Vortex methods have been used extensively in modelling aerodynamic lifting bodies. In marine hydrodynamics a good example of the vortex method is the lifting surface/line theory for a marine propulsor. Vortex methods have also found wide applications in the study of separated flows and in turbulence simulation. A limited number of applications can also be found in the simulation of free surface wave problems. For the many practical applications of vortex methods see the review by Sarpkaya.[1] In turbulence modelling, vortex methods have revealed the inherent instability associated with large-scale coherent vortical structures. In that subject it is generally impossible to avoid the physical instabilities. The free surface flow problem, however, is physically stable as compared to the shear flow problem at high Reynolds number. For this reason it should be much easier to apply a vortex method to the gravity free surface wave flow, which is one of the major considerations of this paper.

Traditionally, because of its complexity, the free surface wave problem was attacked by a linearization of the free surface boundary condition. The formulations can be conveniently

0271–2091/92/111289–22$11.00

Received 2 February 1991
Revised 5 September 1991

classified into Lagrangian or Eulerian according to the methods used to formulate the problem. Solution methods can be divided into integral or differential equation methods, both of which can be conveniently implemented numerically through either finite difference or finite element schemes. A review of the differential equation approaches was given by von Kerczek.[2] A typical approach of the integral equation method uses a distribution of singularities on the body's wetted surface and a Green function that satisfies the linearized free surface boundary condition. In that approach the task of finding the appropriate Green function is tedious and sometimes impossible, especially when the boundary condition is to be satisfied exactly on the exact location of the free surface. Wehausen and Laitone[3] gave an excellent review on this subject.

Recently significant progress has been made on the non-linear free surface problem. Most approaches used the velocity potential. Hunt[4] gave a detailed description of the potential theory used in aerodynamics and hydrodynamics with regard to the existence and uniqueness of the boundary integral methods for incompressible potential flow. Longuet-Higgins and Cokelet[5] formulated the two-dimensional problem in terms of the velocity potential and its derivative and used the formulation to simulate two-dimensional progressing and breaking waves. Greenhow *et al.*[6] formulated a non-linear free surface body–wave interaction problem based also on the velocity potential (see also Reference 7). When compared with experiments, the results are acceptable, although some difficulties were pointed out by the authors. On the other hand, in the application of the vortex method, Zaroodny and Greenberg[8] attempted a non-linear vortex sheet modelling of the free surface and used it to simulate a two-dimensional solitary wave at a finite depth. Zalosh[9] also used a discrete vortex method to simulate the evolution of a two-dimensional interface between two fluids of different densities with the effect of surface tension, though the results were far from perfect. Baker *et al.*[10] used a different approach to the two-dimensional non-linear free surface problem periodic in horizontal co-ordinate x. In that approach dipoles were distributed on the interfaces and the evolution equations established for the complex velocity potential and the dipole strength. The formulation was then tested in the simulation of steady and unsteady two-dimensional surface and interfacial gravity waves with and without bottom topography as well as the resonant interaction of surface and interfacial gravity waves. The results were reported to be good. A similar approach was used by Telste[11] to study the rise of a cylinder to a free surface. In a closely related application, vortex methods have been used to study the instabilities in a stratified fluid (see e.g. References 12 and 13).

This paper demonstrates the applicability and some advantages and flexibilities of a vortex method in solving non-linear free surface problems. In this paper the problem of a two-dimensional body in unsteady translation is first formulated using a vortex sheet model of the free surface. Alternative numerical implementations are discussed. The selected algorithm is tested on the simple case of a two-dimensional circular cylinder in unsteady translation below the free surface in comparison with an approximate linearized analytical solution.

2. FORMULATION OF PROBLEM

2.1. Unsteady motion

In this subsection the formulation will be developed for a two-dimensional body in unsteady translation below or on a free surface formed by water and air in the presence of gravity. It will be assumed that the flow is inviscid, incompressible and irrotational. The surface tension will be neglected. The body will be started from an initial position. The water is infinitely deep. The body can be partially or fully submerged in water while in motion. The necessary governing equations

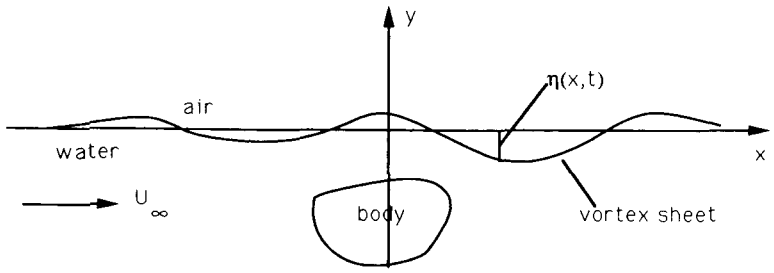

Figure 1. Co-ordinate system

to be satisfied are the following, in a frame fixed on the body (Figure 1):

$$\nabla^2 \Phi^{a,w} = 0, \tag{1}$$

$$\nabla \Phi^{a,w} \cdot \hat{\mathbf{n}} = 0 \quad \text{on} \quad y = s(x), \tag{2}$$

$$p^a = p^w = p \quad \text{on} \quad y = \eta(x, t), \tag{3}$$

$$\frac{d\mathbf{X}}{dt} = \nabla \Phi^w \quad \text{on} \quad y = \eta(x, t), \tag{4}$$

$$\eta(x, 0) = \eta_0, \tag{5}$$

$$\nabla \Phi^{a,w}(x, y, 0) = \nabla \Phi_0^{a,w}, \tag{6}$$

$$\nabla \Phi \equiv \mathbf{V} \equiv \tfrac{1}{2}(\nabla \Phi^a + \nabla \Phi^w) \quad \text{on } y = \eta(x, t), \tag{7}$$

where the superscripts 'a' and 'w' denote air and water respectively, Φ and η are the velocity potential and the surface elevation above the undisturbed position respectively and $\mathbf{X} = x\hat{\mathbf{i}} + \eta(x, t)\hat{\mathbf{j}}$ is the position vector of a point on the free surface.*

If the free surface is replaced by a vortex sheet and the body contour by a source sheet,† and if the limits are taken as the field point approaches the body surface from outside and the free surface from both sides respectively, defining $\nabla \Phi^w - \nabla \Phi^a \equiv \gamma \hat{\boldsymbol{\tau}}$ on $y = \eta(x, t)$ and using the Euler equation in both water and air at the interface in the moving frame fixed on the body, one can derive

$$\rho^w \frac{D\gamma}{Dt} + 2\rho^w \hat{\boldsymbol{\tau}} \cdot \frac{D\mathbf{V}}{Dt} + \rho^w \gamma \left(\hat{\boldsymbol{\tau}} \cdot \frac{\partial \mathbf{V}}{\partial s} + \frac{1}{2} \frac{\partial \gamma}{\partial s} \right) + 2\rho^w g \hat{\boldsymbol{\tau}} \cdot \hat{\mathbf{j}} = -2 \frac{\partial p^w}{\partial s} + 2\rho^w \frac{\partial U_\infty}{\partial t} \hat{\boldsymbol{\tau}} \cdot \hat{\mathbf{i}} \quad \text{on } y = \eta(x, t)_-, \tag{8}$$

$$-\rho^a \frac{D\gamma}{Dt} + 2\rho^a \hat{\boldsymbol{\tau}} \cdot \frac{D\mathbf{V}}{Dt} - \rho^a \gamma \left(\hat{\boldsymbol{\tau}} \cdot \frac{\partial \mathbf{V}}{\partial s} - \frac{1}{2} \frac{\partial \gamma}{\partial s} \right) + 2\rho^a g \hat{\boldsymbol{\tau}} \cdot \hat{\mathbf{j}} = -2 \frac{\partial p^a}{\partial s} + 2\rho^a \frac{\partial U_\infty}{\partial t} \hat{\boldsymbol{\tau}} \cdot \hat{\mathbf{i}} \quad \text{on } y = \eta(x, t)_+, \tag{9}$$

where $\hat{\boldsymbol{\tau}} = \hat{\mathbf{k}} \times \hat{\mathbf{n}}$ is the unit vector locally tangent to the interface, $D/Dt = \partial/\partial t + \mathbf{V} \cdot \nabla$ is the total derivative following the vortex sheet (free surface) and s is the arc length on the free surface.

* The body and the free surface elevation need not have an explicit expression such as $s(s)$ or $\eta(x, t)$ it only serves as a convenient notation. $\hat{\mathbf{n}}$ is a unit normal pointing into the water.

† The body contour should be represented by a vortex sheet in lifting cases.

Equations (8) and (9) can be combined with (3) to give

$$\frac{D\gamma}{Dt}+2\kappa\hat{\mathbf{t}}\cdot\frac{D\mathbf{V}}{Dt}+\gamma\hat{\mathbf{t}}\cdot\frac{\partial\mathbf{V}}{\partial s}+\tfrac{1}{2}\kappa\gamma\frac{\partial\gamma}{\partial s}+2\kappa g\hat{\mathbf{t}}\cdot\hat{\mathbf{j}}=2\kappa\frac{\partial U_\infty}{\partial t}\hat{\mathbf{t}}\cdot\hat{\mathbf{i}}\quad\text{on } y=\eta(x,t), \tag{10}$$

where $\kappa=(\rho^w-\rho^a)/(\rho^w+\rho^a)$ is the density ratio or Atwood number. Equation (10) is a general equation applicable not only to a water–air interface but also to other stratified fluids with arbitrary density ratio κ. For a shear interface in a uniform fluid the vortex density is conserved following a fluid particle, except for stretching of the vortex sheet due to the local non-uniform velocity field, which is represented by the third term in (10).

In passing, it should be mentioned that equation (8) can be used for studying the evolution of a water surface under the action of a prescribed pressure field above the water surface, in which case $\partial p^w/\partial s$ in the equation is known.

Now the other limit of interest, where $p^w\gg\rho^a$, will be explored further by letting $\kappa=1$. This yields

$$\frac{D\gamma}{Dt}+2\hat{\mathbf{t}}\cdot\frac{D\mathbf{V}}{Dt}+\gamma\hat{\mathbf{t}}\cdot\frac{\partial\mathbf{V}}{\partial s}+\frac{\gamma}{2}\frac{\partial\gamma}{\partial s}+2g\hat{\mathbf{t}}\cdot\hat{\mathbf{j}}=2\frac{\partial U_\infty}{\partial t}\hat{\mathbf{t}}\cdot\hat{\mathbf{i}}\quad\text{on } y=\eta(x,t). \tag{11}$$

Equation (11), applicable on the air–water interface, is to be used for updating the free surface vortex strength.

Now define

$$\mathbf{V}=U_\infty\hat{\mathbf{i}}+\mathbf{v}, \tag{12}$$

where $\mathbf{v}$ is the disturbance velocity due to the free surface and body contour singularities; if we use the total derivative following a water particle below the vortex sheet, $D^w/Dt=\partial/\partial t+\mathbf{V}^w\cdot\nabla$, where $\mathbf{V}^w=\mathbf{V}+\gamma\hat{\mathbf{t}}/2$, then equation (11) leads to a simpler form given by

$$\frac{D^w\gamma}{Dt}+2\hat{\mathbf{t}}\cdot\frac{D^w\mathbf{v}}{Dt}+2g\hat{\mathbf{t}}\cdot\hat{\mathbf{j}}=0.$$

This simple equation has clear physical meaning. It states that the time rate of change of vortex density on the sheet is due to the non-linear particle acceleration, which is to be balanced by a restoring term due to gravity. If the above equation is used to update the vortex density on the sheet, it can be seen that the vortex density is first generated by a disturbance represented in a non-uniform velocity field. On initial generation of vortices in the near field the vortices are convected downstream, causing surface elevation. The surface elevation, however, cannot increase arbitrarily but is limited by the restoring term due to gravity. The interplay of the three terms in the above equation accounts fully for the wave mechanics on the free surface. If the above equation is written in a Eulerian frame, the change in vortex density can be explained as due to the time rate of change of the velocity field plus the distortion produced by the non-uniformity of the velocity field. For time stepping, however, the Lagrangian frame seems to be the more convenient implementation.

Our working equations can be summarized as follows:

$$0=U_\infty(t)\hat{\mathbf{i}}\cdot\hat{\mathbf{n}}+\frac{\sigma}{2}+\hat{\mathbf{n}}\cdot PV\int_{y=s(x)}\sigma\nabla G\,ds+\hat{\mathbf{n}}\cdot\int_{y=\eta(x,t)}\gamma\hat{\mathbf{k}}\times\nabla G\,ds\quad\text{on } s(x)_+, \tag{13}$$

$$\mathbf{V}=U_\infty(t)\hat{\mathbf{i}}+\int_{y=s(x)}\sigma\nabla G\,ds+PV\int_{y=\eta(x,t)}\gamma\hat{\mathbf{k}}\times\nabla G\,ds\quad\text{on } y=\eta(x,t) \tag{14}$$

$$\frac{D^w\gamma}{Dt}+2\hat{\tau}\cdot\frac{D^w\mathbf{v}}{Dt}+2g\hat{\tau}\cdot\hat{\mathbf{j}}=0 \quad \text{on } y=\eta(x,t)_-, \tag{15}$$

$$\frac{d\mathbf{X}}{dt}=\mathbf{V}^w \quad \text{on } y=\eta(x,t), \tag{16}$$

$$\eta(x,0)=\mathbf{V}(x,y,0)=0 \quad \text{at } t=0, \tag{17}$$

where $\hat{\tau}=\hat{\mathbf{k}}\times\hat{\mathbf{n}}$, s is the arc length along $\eta(x,t)$ or $s(x)$ and

$$G=\frac{1}{2\pi}\ln\{[(x-\xi)^2+(y-\eta)^2]^{1/2}\}.$$

Here the rest position has been used for simplicity as an initial condition.

It can be seen from the above development that the essential feature of the current formulation is the use of the vortex density instead of the velocity potential in the study of the free surface body–wave interaction problem. This formulation gives clear physical meaning but at the same time introduces two time derivatives into the same equation (15). In a general three-dimensional problem, since the vortex density is a vector on the free surface, the computation procedure will possibly be more involved than the velocity potential formulation. As mentioned in Section 1, some simulations for stratified fluids in the literature have indicated the unstable nature of the interfacial waves. Thus it is interesting to see if the current vortex sheet modelling can avoid instabilities and thus give more easily obtainable and useful results.

Although equation (14) can be substituted into equation (15) to yield an integral equation for the vortex density γ, which can be solved simultaneously with equation (13) for σ, the advantage of doing that is not obvious. First, when the time derivative is taken, there will be an extra term due to the convection of the vortex sheet, making the coupled equations more complicated than they look now. Secondly, the time derivative will make the kernels of the integrals one order more singular than they appear now, so that some special technique is needed to treat the integrals. Thirdly, the integral equations will be simultaneous for both the source density on the body and the vortex density on the free surface. When numerically implemented, the size of the matrix corresponding to the integral equations will be $(N+M)\times(N+M)$ if N source elements on the body and M vortex elements on the free surface are used. That will make it computationally more expensive at each time step than if only the source density is solved from the integral equations whereas the vortex density is obtained from the evolution equations. In this paper an iterative calculation procedure is adopted and will be discussed in more detail in the following sections.

For the steady state ($\partial/\partial t=0$) the free surface velocity is tangential, $\mathbf{V}=V_s\hat{\tau}$, since $\eta(x,t)$ is a streamline. Equation (15) then becomes

$$\frac{\partial}{\partial s}\left[\left(V_s+\frac{\gamma}{2}\right)^2\right]+2g\hat{\tau}\cdot\hat{\mathbf{j}}=0. \tag{18}$$

Equation (11) can also be derived from the Lagrangian derivative of the circulation Γ at the interface of two fluids of different densities by using the Euler equations in the two fluids and the equal pressure condition at the interface.[14] It can be shown that

$$\frac{D\Gamma}{Dt}=\int_a^b -2\kappa\left[g\hat{\mathbf{j}}+\gamma\frac{\partial}{\partial s}\left(\frac{\gamma}{4}\hat{\tau}\right)+\frac{D\mathbf{V}}{Dt}\right]\cdot\hat{\tau}\,ds$$

and

$$\frac{\mathrm{D}}{\mathrm{D}t}(\gamma\hat{\boldsymbol{t}})+\gamma\frac{\partial\mathbf{V}}{\partial s}+2\kappa\left[g\hat{\mathbf{j}}+\gamma\frac{\partial}{\partial s}\left(\frac{\gamma}{4}\hat{\boldsymbol{t}}\right)+\frac{\mathrm{D}\mathbf{V}}{\mathrm{D}t}\right]=0$$

apply on the sheet in the fixed co-ordinate system, where $\kappa=(\rho_2-\rho_1)/(\rho_2+\rho_1)$ and ρ_1 and ρ_2 are the densities of the two fluids. From the above it is easily seen that only when $\rho_1=\rho_2$ is $\mathrm{D}\Gamma/\mathrm{D}t=0$. If $\rho_1\neq\rho_2$, circulation is obviously not conserved along the streakline at the position of the sheet. If $\rho_1=0$, which approximates the air–water interface, $\kappa=1$. When dotted into $\hat{\boldsymbol{t}}$ and written in the moving frame, the above equation becomes identical to the one previously derived. The two different derivations indicate two different approaches to the same problem: one can use either the vortex density or the circulation in the dynamic equation but the latter approach is applicable to two-dimensional problems only.

The working equations (13)–(17) may be non-dimensionalized with

$$\nabla'=L\nabla, \qquad U'_\infty(t')=U_\infty(t)/U_\infty(\infty), \qquad \mathbf{V}'=\mathbf{V}/U_\infty(\infty),$$
$$(\sigma',\gamma')=(\sigma,\gamma)/U_\infty(\infty), \qquad s'=s/L, \qquad (x',y')=(x/L,y/L),$$
$$\eta'=\eta/L, \qquad Fr=U_\infty(\infty)/\sqrt{(gL)}, \qquad t'=tU_\infty(\infty)/L,$$

where L is the body characteristic length and $U_\infty(\infty)=U_\infty(t\to\infty)$.

After the singularity densities have been obtained for the new time step, the pressure on the body can be found from Bernoulli's equation in moving co-ordinates (see Reference 15, p. 89). The expressions are omitted to save space.

2.2. *Steady state structure of far-field downstream vortex sheet*

For steady flow, $\partial/\partial t=0$ and $\mathbf{V}=V_s\hat{\boldsymbol{t}}$ on $y=\eta(x)$. Integration of (18) in s and non-dimensionalization gives

$$V'_s=-\frac{\gamma'}{2}+\sqrt{\left(1-\frac{2\eta'}{Fr^2}\right)}. \tag{19}$$

An important restriction on the free surface elevation implies from this relation:

$$\eta'\leqslant\tfrac{1}{2}Fr^2. \tag{20}$$

This equation states that the maximum achievable wave elevation is restricted by the free stream velocity or by the free stream energy carried by the fluid particles. Note that the linearized Bernoulli equation does not impose an upper bound on the wave elevation.

2.2.1. Stability considerations. Equation (14) can be dotted into $\hat{\boldsymbol{t}}$ and substituted into equation (19) to yield an equation for the vortex density γ' in the steady state:

$$\gamma'=-2\hat{\boldsymbol{t}}\cdot\hat{\mathbf{i}}+2\sqrt{\left(1-\frac{2\eta'}{Fr^2}\right)}-2\hat{\boldsymbol{t}}\cdot\int_{y'=s'}\sigma'\nabla'G'\,\mathrm{d}s'-2\hat{\boldsymbol{t}}\cdot PV\int_{y'=\eta'}\gamma'\hat{\mathbf{k}}\times\nabla'G'\,\mathrm{d}s' \text{ on } y'=\eta'(x',t'). \tag{21}$$

For simplicity consider the far-field approximation of equation (21) in which the contributions from the source distribution (far away) and vortex distribution (mostly perpendicular to the sheet, assuming small wave elevation) can be effectively neglected. Further assume

$$\eta',\frac{\partial\eta'}{\partial x'}\sim\varepsilon, \qquad u',v',\gamma'\sim\varepsilon, \qquad \hat{\boldsymbol{t}}\cdot\hat{\mathbf{j}}=\sin\alpha\sim\frac{\partial\eta'}{\partial x'}\sim\varepsilon, \qquad \hat{\boldsymbol{t}}\cdot\hat{\mathbf{i}}=\cos\alpha\sim1,$$

where u' and v' are the components of the non-dimensional disturbance velocity vector and $\lim \varepsilon=0$. Then a linearization can be made as follows:

$$\begin{aligned}\gamma' &\approx -2\hat{\mathbf{t}}\cdot\hat{\mathbf{i}}+2\sqrt{\left(1-\frac{2\eta'}{Fr^2}\right)}\\ &\approx -\frac{2}{\sqrt{[1+(\partial\eta'/\partial x')^2]}}+2\left(1-\frac{\eta'}{Fr^2}\right)\\ &\approx \left(\frac{\partial\eta'}{\partial x'}\right)^2-2\frac{\eta'}{Fr^2}\\ &\approx -2\frac{\eta'}{Fr^2}.\end{aligned} \tag{22}$$

This linearization shows that γ' is positive whenever η' is negative and vice versa. This is different from the situation arising from a disturbed vortex sheet in a uniform flow of uniform density, in which case it can be shown that the sheet is unconditionally unstable (the Kelvin–Helmholtz instability). The above is more analogous to the discrete vortex street analysed by von Karman many years ago. A von Karman vortex street has an alternating sign characteristic similar to that observed here. The von Karman vortex street is stable if it has a certain structure (e.g. the ratio of the vertical distance to the horizontal distance between point vortices being 0·281). Similarly we may expect the vortex sheet in our problem to have a stable structure which dictates the wavelength of the far-field wave downstream. The stability should be neutral in the same sense as for a von Karman vortex street, in which too large a disturbance to the structure (e.g. numerical errors) could destroy the stability.

Consider the interface of two fluids of different densities moving with speed $U/2$ in opposite directions one on top of the other. It can be shown (see Reference 16, pp. 373–374 and 461–462) that the characteristic solution of the amplitude of the interface is

$$r=-\frac{\mathrm{i}}{2}U\alpha\kappa\pm\frac{1}{2}U\alpha\sqrt{\left(1-\kappa^2-\frac{2}{\pi}\frac{\kappa}{Fr_\lambda^2}\right)},$$

where $\alpha=2\pi/\lambda$, λ is the wavelength of the disturbance, $Fr_\lambda=U/\sqrt{(g\lambda)}$ is the Froude number based on the disturbance wavelength and κ is the density ratio. From this expression it can be seen that when $\kappa\leqslant 0$, which corresponds to the heavy fluid above, the solution is always unstable. When $0<\kappa<1$, the solution is unstable for large Fr_λ or small wavelength λ as compared to U. When $\kappa=1$, the stability is neutral in the sense that a slight change in the density could introduce instability. Numerical errors could mimic the slight density difference and could therefore adversely affect calculations. This is probably the reason why some numerical disturbances were found in some of the early free surface simulations.

The above linearized stability analysis result is from a solution using separation of variables. The conclusion of the neutral stability can be conveniently used here to study the structure of the far-field vortex sheet downstream.

For the steady state the linearized equation for γ' far downstream has been given previously by (22) as

$$\gamma'\approx -\frac{2\eta'}{Fr^2}, \tag{23}$$

where all variables are non-dimensionalized.

For simplicity we ignore all upstream influence and consider now a sinusoidal wave form without the presence of the body, i.e.

$$\eta' = \eta'_0 \sin(\alpha\xi + \theta). \tag{24}$$

Here x, y, ξ and η are the non-dimensional variables, η' is the wave elevation and η is an integration variable. The disturbance velocity on the vortex sheet can be written as

$$\mathbf{v}' = \frac{1}{2\pi} \int_{\text{sheet}} \frac{[(x-\xi)\hat{\mathbf{j}} + (\eta - y)\hat{\mathbf{i}}]\gamma'(s)\,ds}{(x-\xi)^2 + (y-\eta)^2}.$$

Assume the wave elevation to be small so that the disturbance velocity can be approximately calculated on the x-axis:

$$\mathbf{v}' \approx \frac{\hat{\mathbf{j}}}{2\pi} \int_{-\infty}^{\infty} \frac{\gamma'(\xi)\,d\xi}{x-\xi}. \tag{25}$$

Substitute (23) and (24) into (25) to give

$$\mathbf{v} = -\frac{\hat{\mathbf{j}}\eta'_0}{\pi Fr^2} \int_{-\infty}^{\infty} \frac{\sin(\alpha\xi + \theta)\,d\xi}{x-\xi}$$

$$= \hat{\mathbf{j}} \frac{\eta'_0}{Fr^2} \cos(\alpha x + \theta).$$

The non-dimensionalized total velocity on the sheet is

$$\mathbf{V}' = \hat{\mathbf{i}} + \mathbf{v}'.$$

The direction of the linearized velocity is given by

$$\tan\alpha_1 = \tan[\arg(\mathbf{V}')] = \frac{\eta'_0}{Fr^2} \cos(\alpha x + \theta).$$

Now this direction of the velocity is compared with the direction of the wave elevation tangent given by

$$\tan\alpha_2 = \frac{d\eta'}{dx} = \alpha\eta'_0 \cos(\alpha x + \theta).$$

To have the steady state wave form in the moving frame we take the *neutral stability* case given by

$$\| \tan\alpha_1 \| = \| \tan\alpha_2 \|$$

or

$$\alpha = \frac{1}{Fr^2}. \tag{26}$$

Thus the far-field downstream wave is given by

$$\eta' = \eta'_0 \sin\left(\frac{1}{Fr^2} x + \theta\right). \tag{27}$$

The wave number α obtained from the above linearized stability analysis, (26), is therefore identical to that of the linearized solution, although it was arrived at from considerations of a linearization of the non-linear vortex sheet model.

2.2.2. Frequency analysis. In the above stability analysis the far-field wave was assumed sinusoidal. This assumption can now be verified by the following simple frequency analysis on the linearized equations. Again the following assumptions are made to linearize the equations:

$$\eta, \frac{\partial \eta}{\partial x} \sim \varepsilon, \qquad u, v, \gamma \sim \varepsilon, \qquad \hat{\boldsymbol{\tau}} \cdot \hat{\mathbf{j}} = \sin\alpha \sim \frac{\partial \eta}{\partial x} \sim \varepsilon, \qquad \hat{\boldsymbol{\tau}} \cdot \hat{\mathbf{i}} = \cos\alpha \sim 1,$$

where u and v are the components of the disturbance velocity vector and ε is a small parameter. With the above assumptions the steady state form of the dynamic boundary condition (15) can be linearized to give

$$U_\infty \frac{\partial \gamma}{\partial x} + 2U_\infty \frac{\partial v_x}{\partial x} + 2g \frac{\partial \eta}{\partial x} = 0.$$

The induced velocity on the x-axis due to the disturbance of a body and a distribution of vortices on the x-axis is

$$v_x = \hat{\mathbf{i}} \cdot \mathbf{v}_b = v_{bx},$$

$$v_y = \hat{\mathbf{j}} \cdot \mathbf{v}_b + \frac{1}{2\pi} \int \frac{\gamma \, d\xi}{x - \xi} = v_{by} + \frac{1}{2\pi} \int \frac{\gamma \, d\xi}{x - \xi},$$

where $\mathbf{v}_b$ is the velocity due to the disturbance of the body alone. The steady state linearized kinematic boundary condition takes the familiar form

$$v_y = U_\infty \frac{\partial \eta}{\partial x}.$$

The above four equations can be combined to give

$$U_\infty \frac{\partial \gamma}{\partial x} + 2U_\infty \frac{\partial v_{bx}}{\partial x} + \frac{2g}{U_\infty} v_{by} + \frac{g}{\pi U_\infty} \int \frac{\gamma \, d\xi}{x - \xi} = 0. \tag{28}$$

Let

$$f(x) = 2U_\infty \frac{\partial v_{bx}}{\partial x} + \frac{2g}{U_\infty} v_{by}.$$

Define the Fourier transforms

$$\bar{\gamma}(\omega) = \frac{1}{2\pi} \int_{-\infty}^{\infty} \gamma(x) e^{-i\omega x} \, dx, \qquad \bar{f}(\omega) = \frac{1}{2\pi} \int_{-\infty}^{\infty} f(x) e^{-i\omega x} \, dx.$$

Then equation (28) can be written as

$$\int_{-\infty}^{\infty} \left[iU_\infty \left(\omega - \frac{g}{U_\infty^2} \right) \bar{\gamma}(\omega) + \bar{f}(\omega) \right] e^{i\omega x} \, d\omega = 0,$$

from which we obtain

$$\bar{\gamma}(\omega) = \frac{i}{U_\infty (\omega - g/U_\infty^2)} \bar{f}(\omega).$$

This equation shows that $\gamma(x)$ has a dominant frequency component given by $\omega = g/U_\infty^2$, which, if non-dimensionalized, is $1/Fr^2$. This verifies our previous assumption on the far-field sinusoidal wave form and the linearized stability analysis. Our previous conclusion about the neutral

stability of the vortex sheet in this particular case has also been confirmed. It is also obvious from the above analysis that the linearized far-field equations cannot be used to obtain a unique far-field wave height. In fact the far-field wave height has to be determined from the analysis of the near field, where the disturbance of the body plays a dominating role. This is consistent with the physical process of the problem.

It should be noted that if U_∞ is changed into c, the celerity of a progressing wave train, the above analysis is also valid for a progressing sinusoidal wave without the presence of a body, in a frame moving at the wave celerity, in which the wave form is steady. In that case, since ω is the wave number, the above results yield a dispersion relation

$$\omega=\frac{2\pi}{\lambda}=\frac{g}{c^2},$$

i.e.

$$c=\sqrt{\left(\frac{g\lambda}{2\pi}\right)},$$

which agrees with the classical linearized Airy wave theory.

3. NUMERICAL ALGORITHM FOR UNSTEADY FLOW

Equations (13)–(17) are used to solve for the unknowns σ on $s(x)$, $\mathbf{V}$ and γ on $\eta(x, t)$ and the free surface elevation $\eta(x, t)$ itself. Owing to the fact that $D^w\gamma/Dt$ and $D^w\mathbf{v}/Dt$ occur in the same equation in (15), the solution procedure involves an iteration, i.e. first a trial iteration for one of the two total derivatives, say $D^w\mathbf{v}/Dt$, then a time stepping for $D^w\gamma/Dt$.

The solution procedure is summarized as follows:

1. For a given $U_\infty(t)$ start from rest or some other prescribed initial condition.
2. Discretize the body contour and the free surface. Assume that (the discrete values of) σ^k on $s(x)$, $\mathbf{V}^k$ and γ^k on $\eta(x, t)$ and $\eta(x, t)$ at current time t or time step k are available.
3. For time step $k+1$ move (the control points of) the vortex sheet with $\mathbf{V}^k$ to the new position according to equation (16).
4. Find the velocity $\mathbf{V}^{k+1}$ at the new position (of the control points of the free surface vortex elements) due to γ^k and σ^k using equation (14). For preparation of step 5 let $\gamma^{k+1}=\gamma^k$ as a first approximation.
5. Solve for (discretized) σ^{k+1} on the body contour using equation (13) with γ^{k+1} known on the free surface.
6. Solve for $\mathbf{V}^{k+1}$ due to σ^{k+1} on the body and γ^{k+1} on the free surface using equation (14).
7. Use $\mathbf{V}^{k+1}$ and $\mathbf{V}^k$ to approximate $D^w\mathbf{v}/Dt$ in equation (15) and check for convergence. If convergence is reached, go to step 9; otherwise, go to step 8.
8. Solve for γ^{k+1} on the free surface from equation (15); go to step 5.
9. Redistribute the sheet to make the sheet vortex elements equally spaced again. (The redistribution algorithm will be described later.)
10. Interpolate γ^{k+1} onto the new sheet. This involves a two-step interpolation: first, right after convection, an interpolation from the control points to the end points of the redistributed panels; secondly, from the end points of panels to the new panel midpoints. Parabolic interpolation is used here although higher-order interpolation is also easy to implement.
11. Find $\mathbf{V}^{k+1}$ at the new sheet position due to σ^{k+1} and γ^{k+1} at the new sheet position. Note that these are the corrected values for the previous approximation, step 6. Go back to step 3 and proceed to the next time step.

In the above iteration, steps 3–8 form an outer loop for one time step for the Lagrangian time derivative $D^w\gamma/Dt$ in (15), while steps 5–8 form an inner iteration loop for $D^w\mathbf{v}/Dt$ in the same equation. Only when the convergence for $D^w\mathbf{v}/Dt$ is satisfied does the iteration go to the outer loop for the next time step. Analysis of the simulation results shows that step 5 in the inner iteration may be skipped after the first inner iteration in most cases since the change in source densities is usually small. For the time steps after the first a reasonable starting point for $D^w\mathbf{v}/Dt$ is the backward difference obtained from the current and previous time steps. In step 9 the reason for the redistribution is mainly to effectively avoid concentration of element control points in certain portions of the sheet, as would be caused by the non-uniform velocity field. For a two-dimensional floating body, in particular, the redistribution can avoid spatial resolution being lower and lower with increasing time on the downstream side of the free surface very close to the body contour owing to the presence of a nearby stagnation point. (Sometimes, however, the non-uniform distribution of control points may be desirable, e.g. in the study of breaking waves where a body is not present.) Another advantage of the redistribution is its stabilizing effect on local small-scale disturbances which were found in some numerical simulations of free surface gravity waves (see e.g. References 5, 11 and 17). There is, however, a trade-off for the redistribution of the sheet. With the redistribution step, higher-order finite difference methods become expensive to implement. Since redistribution of the control points on the sheet involves a numerical interpolation, the order of interpolation must be consistent with the order of time stepping if a higher-order scheme is to be used. The exact effect on the accuracy of the procedure is to be further investigated. There is an alternative way to implement the above algorithm, i.e. by using a fixed grid and interpolating everything onto the grid, then interpolating quantities back from the grid when each is needed at control points of the elements.[18] That approach can be expected to achieve possibly a higher accuracy at the expense of generating undesired grid effects. The exact amount of the trade-off is also to be explored further in the future.

In the current implementation of the above algorithm, uniform strength source and vortex elements are used. Theoretically there is a discontinuity in the velocity across a vortex sheet. To avoid numerical difficulties, a thin shear layer is constructed to represent this discontinuity so that the velocity will never be singular anywhere in the domain, not even at the two ends of a vortex panel where a logarithmic singularity is normally expected. The velocity in the thin shear layer is assumed to be a linear distribution, continuous from the outer velocity field. Both equations (15) and (16) are discretized by a first-order forward difference Euler scheme in a Lagrangian frame, i.e. the time derivative is the one that follows the fluid particles on the sheet.

The redistribution procedure is as follows (shown in Figure 2). Assume $a, b, c, d, \ldots$ are the middle points of elements after one time step. Assume that $A, B, C, D, \ldots$ are equally spaced points on the sheet with spacing between any two successive points equal to l, say. If one starts from point a, then one first checks $|ab|$: if $|ab| \geqslant l$, get point B on ab such that $|AB| = l$; otherwise, get B on bc such that $|AB| = l$. The same procedure is followed for $C, D, \ldots$. Since $A, B, C, D, \ldots$

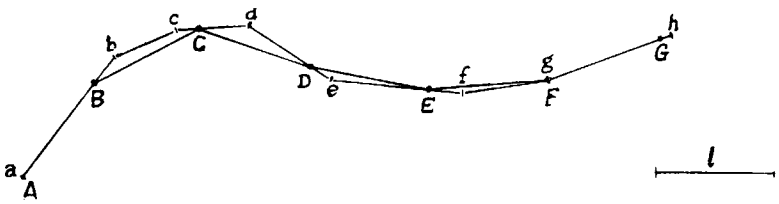

Figure 2. Redistribution of control points on sheet in one time step

are on the lines ab, bc, . . . , the interpolation of vortex density from a, b, c, d, . . . is straightforward. A, B, C, D, . . . can be taken as end points of the new elements. Then the middle points are obtained by averaging and the vortex densities on the middle points are parabolically interpolated from those of the end points.

To save computation cost, the vortex density far away may be lumped into equivalent point vortices and several point vortices can be combined into an equivalent one with equivalent circulation and location as used by Deffenbaugh and Marshall[19] and Porthouse and Lewis,[20] which is also similar to the subvortex technique used by Maskew.[21] Due to the non-linearity of the induced velocity field, the equivalence is only approximate and not uniform with location. However, that approximation does offer a convenient way to cut down substantially the computational cost for high resolution associated with short waves.

4. RESULTS AND DISCUSSION: UNSTEADY TRANSLATION OF A SUBMERGED CIRCULAR CYLINDER

The numerical solution procedure in Section 3.1 is tested for a circular cylinder in unsteady translation below a water–air free surface. In the current simulations the iteration for dv/dt as outlined in the previous section converges relatively fast. For a convergence criterion (based on the sum of the relative error of the velocities at all control points of free surface panels) of 0·01, it takes less than five iterations for all cases. The simulation results are shown in Figures 3–11. The free surface elevation is plotted in the moving frame. The centre of the cylinder is located at $x=0$ and $y=-f$, where f is the submergence of the cylinder. It is started from the still position with a uniform acceleration until it reaches a steady speed (which is equivalent to a time-varying free stream starting from rest with a uniform acceleration in the moving frame). The Froude number is based on the ultimately achieved *steady* free stream speed (or the maximum translational speed of

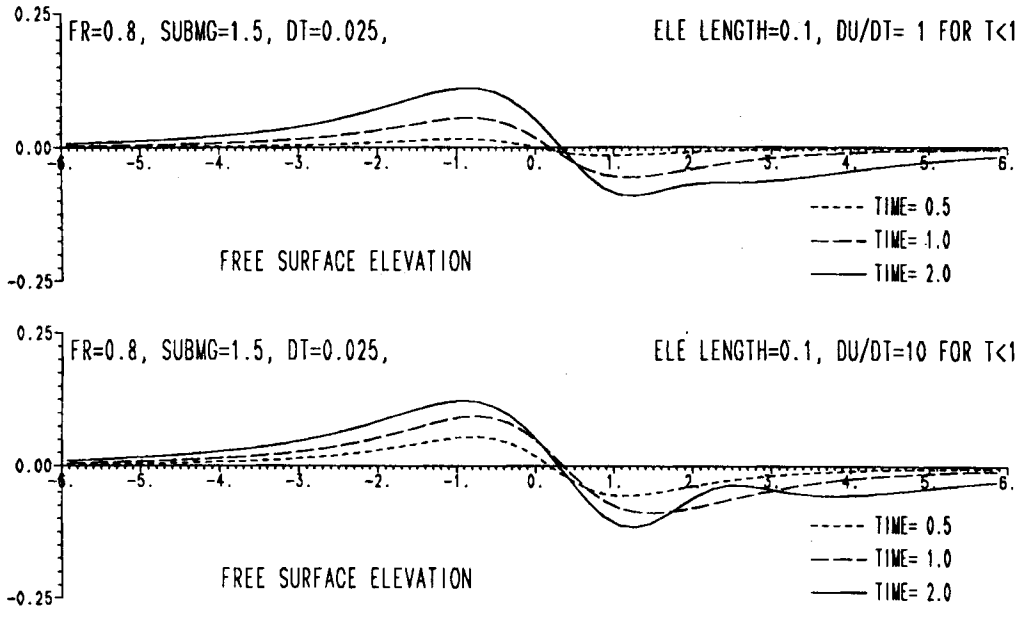

Figure 3. Evolution of free surface elevation due to a submerged circular cylinder in unsteady translation to the left; Froude number 0·8, submergence 1·5, different initial accelerations

the cylinder) and the body diameter. Different submergences, Froude numbers and accelerations are tested (the submergence being the distance from the centre of the cylinder to the undisturbed free surface). The quantities shown in the figures are non-dimensional. In the numerical calculations the body, with a radius of 0·5, is divided into 36 panels with constant source density on

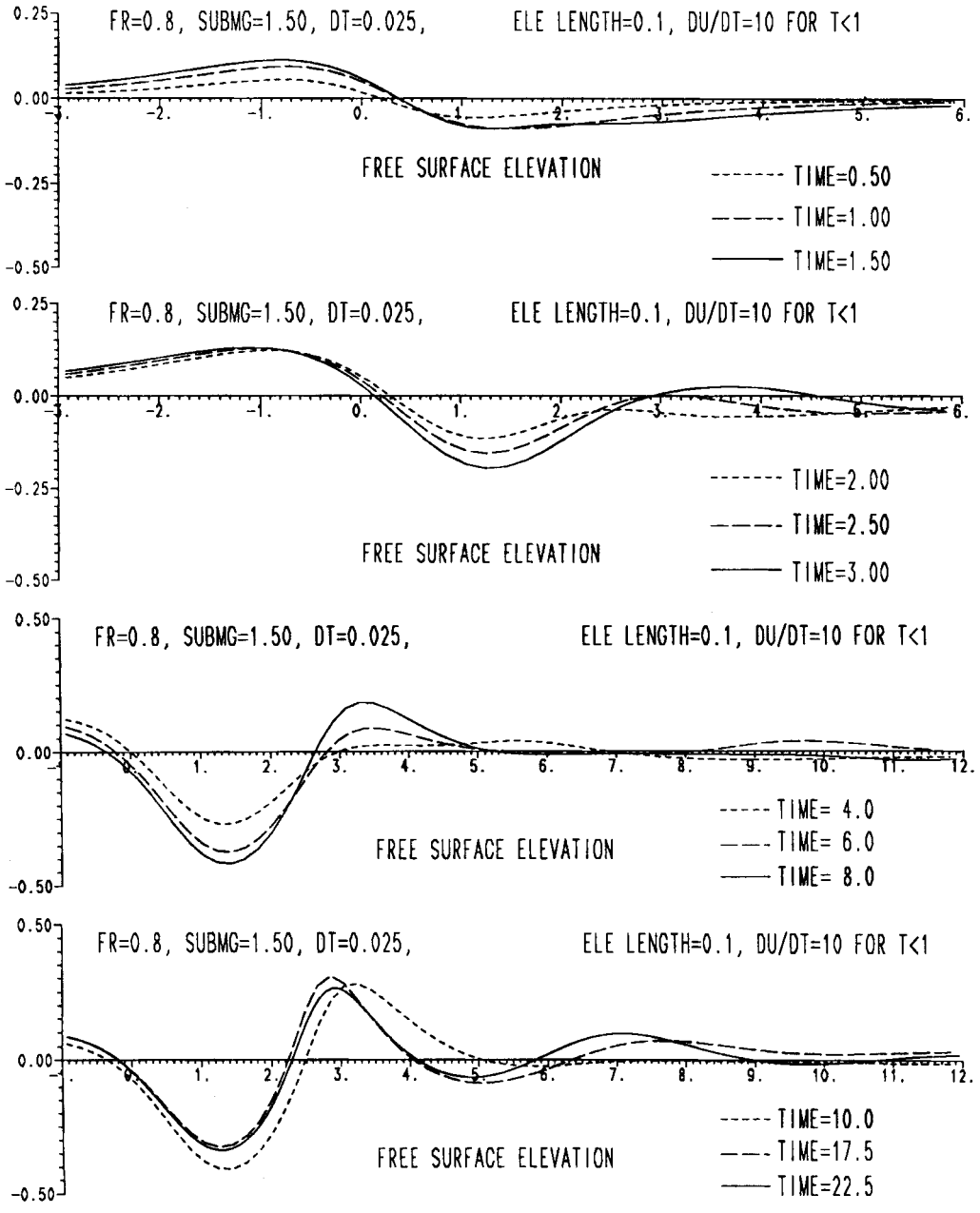

Figure 4. Evolution of free surface elevation due to a submerged circular cylinder in unsteady translation to the left; Froude number 0·8, submergence 1·5, initial acceleration 10

each panel. The free surface is modelled with constant density vortex panels, each of which is 0·1 in length. The time step size is chosen to be 0·025. The infinite free surface is cut at a distance of 9 upstream and 18 downstream for numerical computations. (The truncation boundary should be compatible with the period of simulation so that no significant errors will be generated from the boundary.)

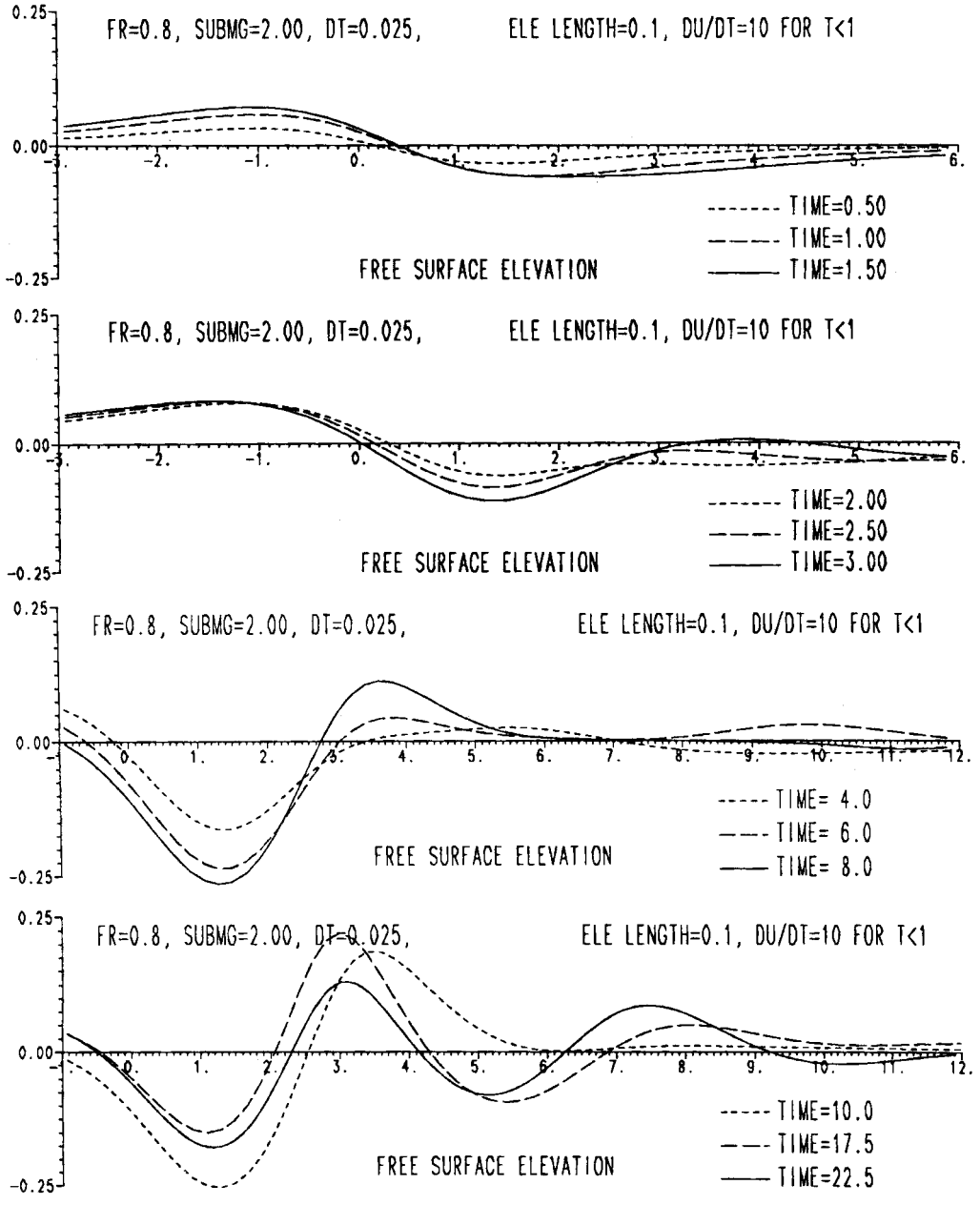

Figure 5. Evolution of free surface elevation due to a submerged circular cylinder in unsteady translation to the left; Froude number 0·8, submergence 2·0, initial acceleration 10

Figure 3 shows the free surface evolution for a steady free stream Froude number equal to 0·8, a submergence equal to 1·5 and initial uniform accelerations of 1·0 and 10·0. Only the results at the early time steps are shown since the difference in later time steps due to the different initial acceleration of the body is not significant. Figure 4 gives a more complete surface evolution for a

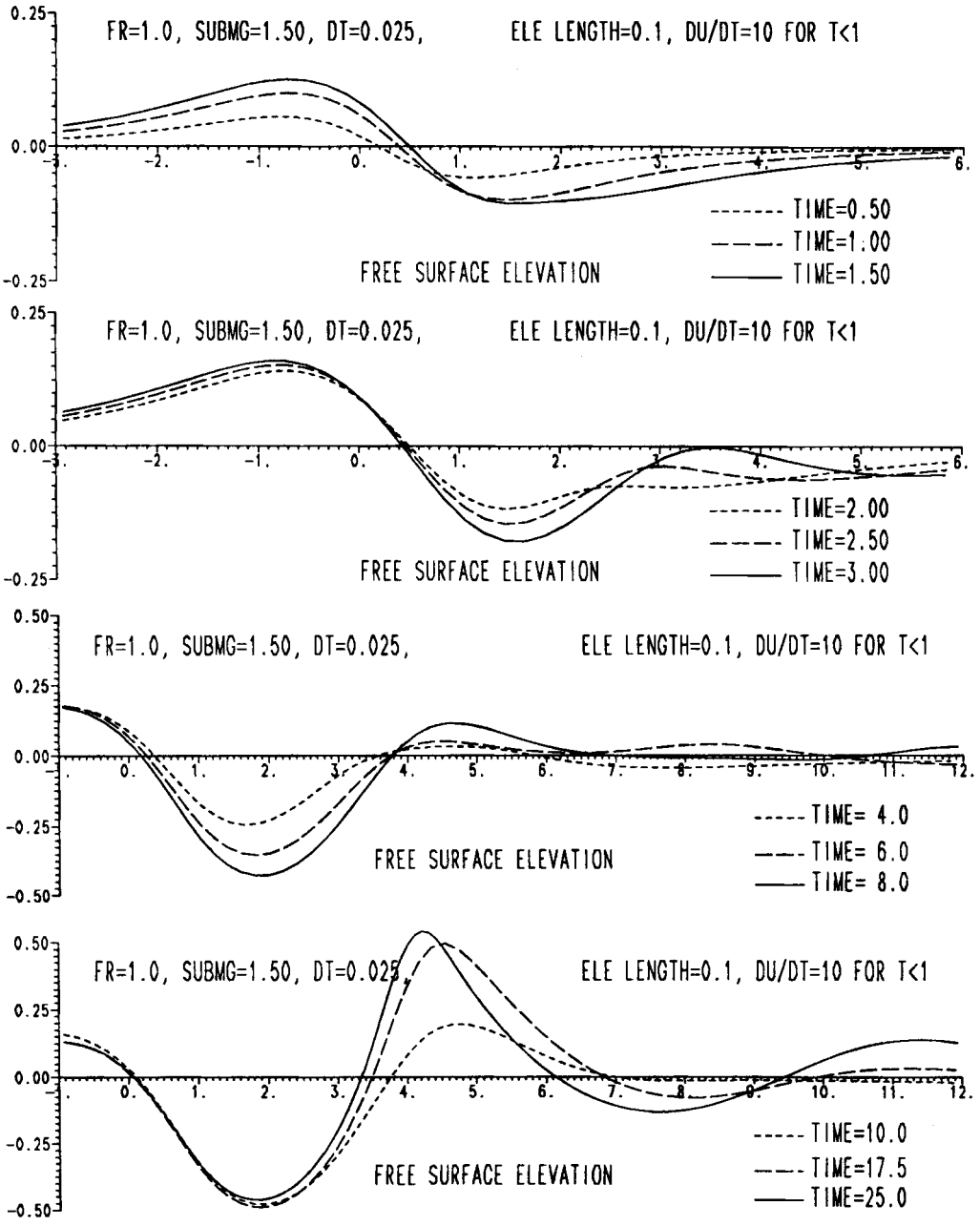

Figure 6. Evolution of free surface elevation due to a submerged circular cylinder in unsteady translation to the left; Froude number 1·0, submergence 1·5, initial acceleration 10

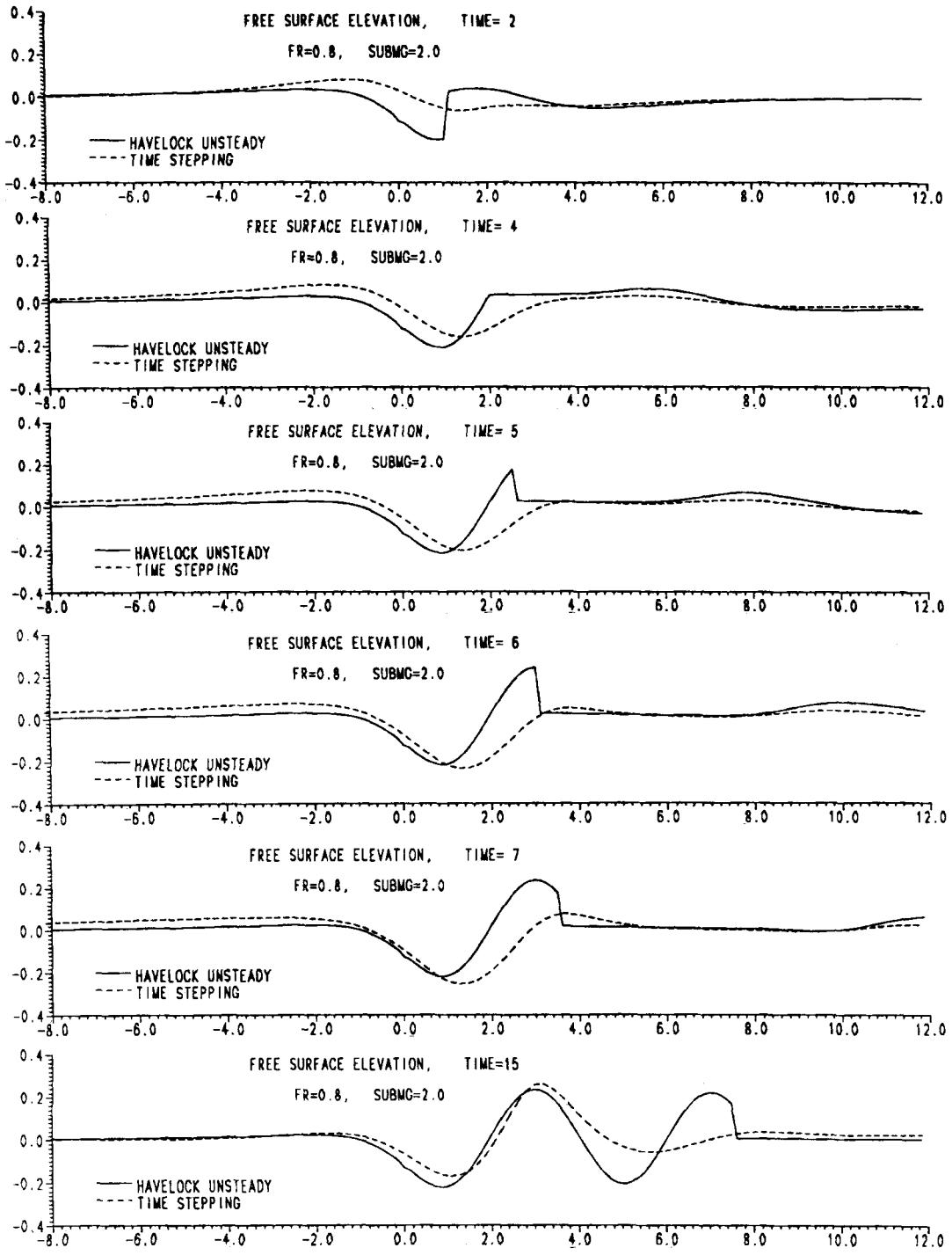

Figure 7. Evolution of free surface elevation due to a submerged circular cylinder in unsteady translation to the left, as compared with linearized approximate solutions by Navelock;[22] Froude number 0·8, submergence 2·0, initial acceleration 10

Froude number equal to 0·8, a submergence of 1·5 and an initial uniform acceleration of 10 until steady speed is achieved. Figures 5 and 6 show the evolution of the free surface (in the body-fixed frame) for different combinations of Froude numbers and submergences. Figure 7 shows a comparison of the unsteady free surface elevation with an approximate linear solution given by Havelock.[22]

The following features can be observed from the simulation results. With increasing submergence the free surface disturbance gets smaller. For the smaller Froude number (Figures 4 and 5) the first trough is closer to the body. It is deep in contrast to the low upstream surface elevation. For the higher Froude number (Figure 6) the motion of the body generates higher surface elevations upstream and above the body. This larger disturbance is attributed to a larger amount of input free stream energy corresponding to the higher Froude number. Another obvious feature is the greater range of the influence of the body, e.g. the deep trough behind the body goes farther downstream as the Froude number increases. Also, the first crest downstream is observed at a later time as the Froude number increases, which is expected since the downstream wavelength is proportional to the square of the Froude number, as shown in the steady motion analysis. Aside from the amplitude, the shape of the near-field non-linear surface elevation is similar for different submergences. When the initial uniform acceleration is changed from $dU_\infty/dt = 1$ to $dU_\infty/dt = 10$ in Figure 3 (corresponding more to an impulsive start), the difference in the shape of the surface elevation is actually minimal, whereas a fast-moving wave due to initial disturbance is more obvious (Figure 5, third frame for $t = 4$–6) and the steady state will be reached sooner.

An interesting aspect to be noticed (in the third frames of Figures 4–6) is that the simulation shows the dispersion due to the initial start of the cylinder. On the downstream side, small-amplitude waves are seen to travel faster than the steady state wave as predicted by the linearized theory.[22] In all cases a faster-moving wave, which is due to the initial set-up of the disturbed near field and the acceleration effect, can be observed to travel downstream after $t = 4$. This wave travels faster than the group velocity, which is equal to half the translational velocity of the cylinder. Actually, the wave crest is a superposition of many small-amplitude waves with wavelengths longer than the steady state wavelength. On approaching steady flow in the near field, this superposition of long waves will be expected to have travelled far downstream and have disappeared from the near field. At $t = 8$ this wave has already travelled out of the frame shown in Figures 4–6. Then the steady dowstream wave which travels at the group velocity will be gradually established. This dispersion has also been observed in the upstream direction (although not shown in the figures), especially when the Froude number is small. In the comparison with the linear approximate solution given by Havelock, the speed of travel of the faster wave due to the initial disturbance is predicted very well by the current simulation (see Figure 7). In that figure there is a discontinuity in surface elevation of the linear solution because Havelock formulated the problem for a cylinder started *suddenly* from the rest position and then made to move at constant speed. The unrealistic formulation introduces a shock at $t = 0$ and the shock is then preserved and propagated at the group velocity. Except for this subtle difference between the linear solution and the current simulation, the overall agreement is acceptable, especially with regard to the small fast wave due to the initial disturbance. (Note that in Havelock's *linear* solution the body boundary condition was *not* imposed.) The above observations are in qualitative agreement with a summary given by Havelock,[22] which, based on the linearized theory, stated that the surface elevation at any time is made up of three parts: (i) the local disturbance travelling with the cylinder, (ii) a regular train of waves behind the cylinder extending from $x = 0$ to $x = \frac{1}{2}U_\infty$ in the moving frame and (iii) a disturbance which spreads out in both directions and diminishes in magnitude as time progresses. In the figures mentioned above it can be seen easily that the first wavelength downstream approaches asymptotically the steady state

wavelength ($1/Fr^2$ non-dimensionalized) as time increases. Before passing, it should be mentioned that the early time history of the surface elevation is also in qualitative agreement with the limited results of a non-linear simulation by Teles da Silva and Peregrine,[23] even though their results were not complete enough for a detailed quantitative comparison. Baker *et al.*[17] also presented some limited results of a numerical simulation of a circular cylinder started impulsively from rest and reported that wave breaking was observed in their numerical experiment. The same parameters were tested with the current numerical simulation procedure. No wave breaking was observed.

Figures 8 and 9 show the wave resistance coefficient as a function of time for a submergence equal to 1·5 and for Froude numbers of 0·8 and 1·0. As a comparison the resistance curves given

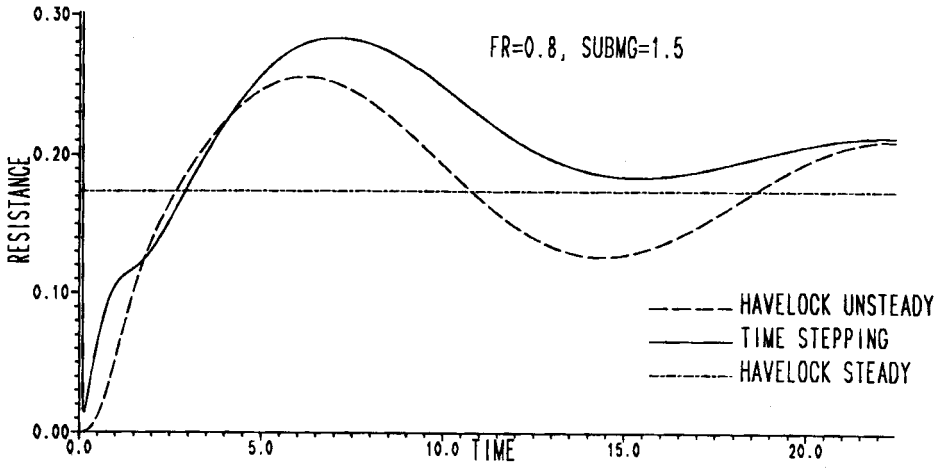

Figure 8. Resistance coefficient versus non-dimensional time for a submerged circular cylinder in unsteady translation to the left; Froude number 0·8, submergence 1·5, initial acceleration 10

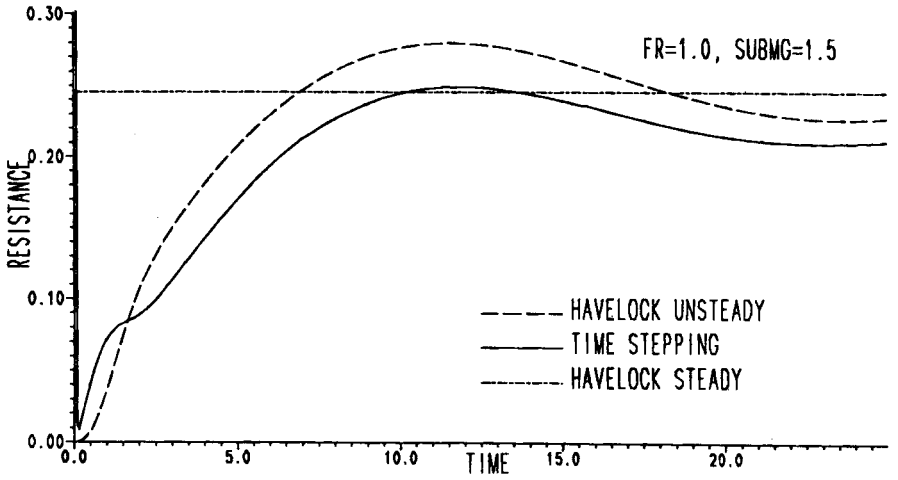

Figure 9. Resistance coefficient versus non-dimensional time for a submerged circular cylinder in unsteady translation to the left; Froude number 1·0, submergence 1·5, initial acceleration 10

by Havelock's linearized approximate solution[22] are also plotted. As can be seen, the agreement is generally very good, especially for the variation of the curves as a function of time. Specifically, Havelock's results show an oscillation of the resistance about the steady state value with a period of oscillation approximately equal to four times the steady wavelength. That behaviour of the resistance has been simulated approximately for about one period of oscillation as shown in the figures. The agreement for Froude numbers equal to 0·8 and 1·0 and a submergence of 2·0 is similarly good but the results are omitted to save some space.

In Figure 10 the cylinder was first started from rest with a uniform acceleration of 1·0 until the steady speed was reached. The speed was then kept constant until a non-dimensional time equal to 5·0 (which corresponds to a distance of five times the diameter of the cylinder travelled by the cylinder in the fixed inertial frame) and then reduced with a constant deceleration of $-1{\cdot}0$ until

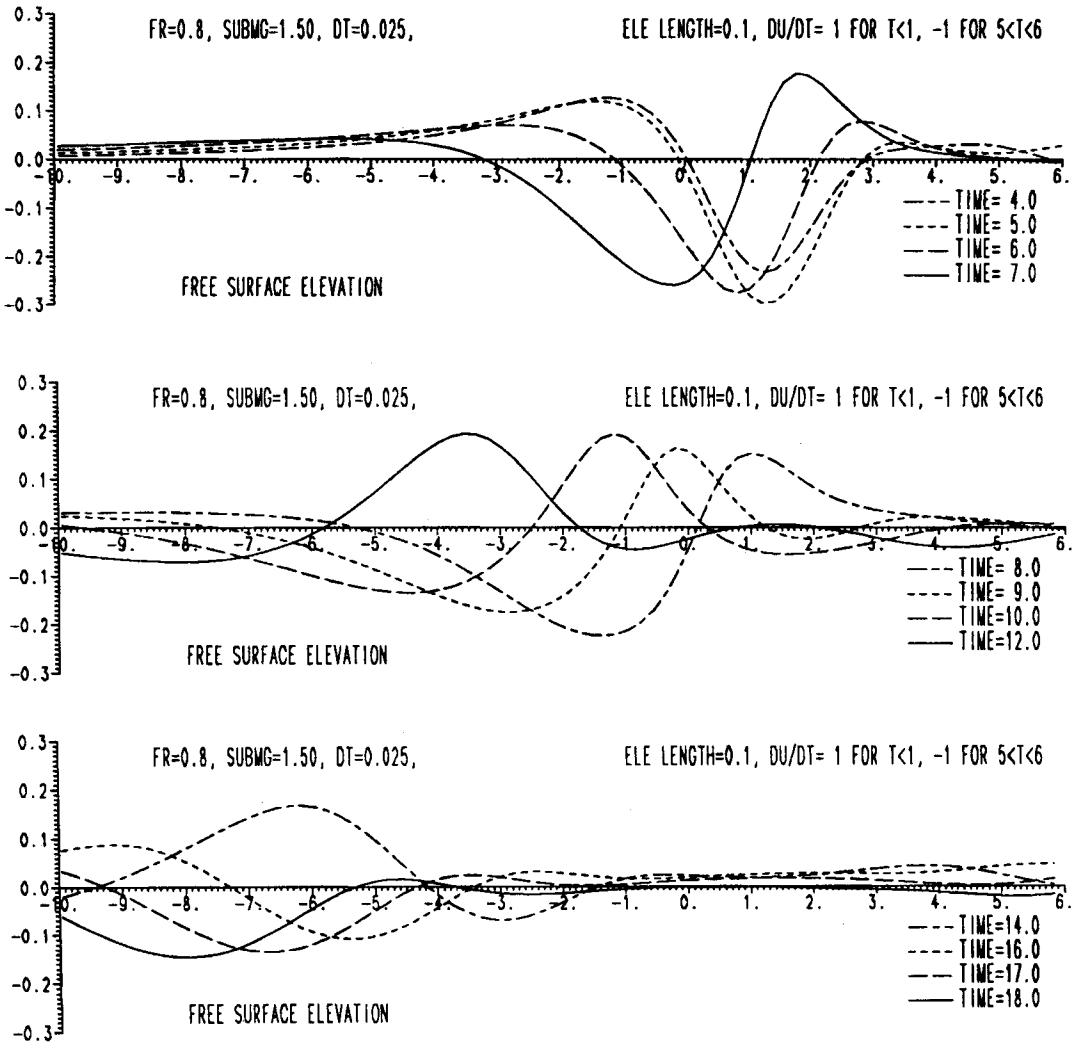

Figure 10. Evolution of free surface elevation due to a submerged circular cylinder in unsteady translation to the left; Froude number 0·8, submergence 1·5, varying acceleration

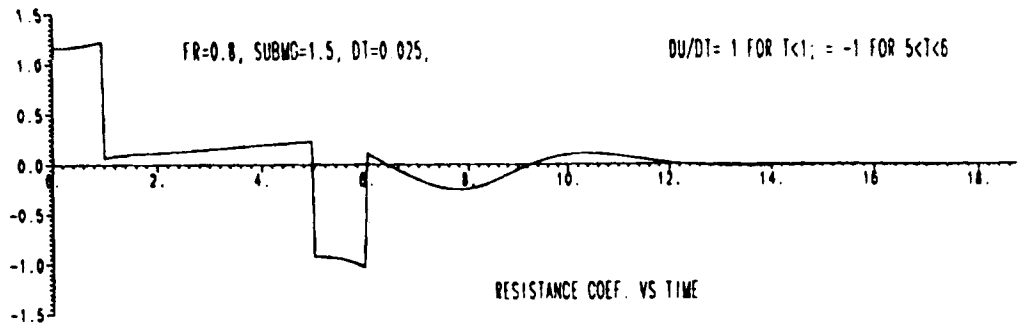

Figure 11 Resistance coefficient versus non-dimensional time for a submerged circular cylinder in unsteady translation to the left; Froude number 0·8, submergence 1·5, varying acceleration

the cylinder came to a complete stop when the translational speed reached zero. The surface elevation shows an interesting process of the downstream wave travelling upstream and gradually overtaking the body and then diminishing in both directions. In the body-fixed frame (the centre of) the cylinder is still located at (0, −1·5). The resistance curve for this case (Figure 11) shows positive resistance at first and then negative resistance due to deceleration and finally a gradual return to zero. The large value of resistance during acceleration and deceleration is obviously due to the added mass effect.

5. CONCLUSIONS

A vortex method for the free surface wave problem has been formulated and numerically implemented to simulate the two-dimensional non-linear body–wave interaction problem. The formulation offers another view to the physical process of the free surface wave problem. It uses the vortex density instead of the velocity potential as a time-stepping variable and uses an iteration scheme on the dynamic boundary equation on the sheet. Numerical simulations have demonstrated the applicability of this vortex method to the practical free surface problem. The stability of such a vortex sheet modelling has also been investigated. It has been shown that a vortex sheet as used to represent a free surface is neutrally stable and that the condition of neutral stability can be used in a linearization of the vortex sheet model to recover its far-field structure as predicted by classical linearized potential theories. Because of the stabilizing effect of the redistribution of the free surface vortices, small-scale instabilities reported by some other investigators were not found with the current method. The current method is particularly suitable for studying non-linear unsteady interactions such as the body–wave interaction and body–wake–wave interaction problems. If an appropriate Kutta condition is used, the method can be easily adopted to simulate the flow past a lifting foil near the free surface, as has been studied by Salvesen and von Kerczek[24] with both a finite difference method and model tests. It can also be easily extended to three dimensions. In three-dimensional applications, however, the scalar vortex density will be replaced by a vector vortex density on the sheet (free surface), making it more difficult to implement numerically. The current method offers certain desired flexibility in dealing with floating bodies without too much difficulty (the simulation results will be presented separately). The method is capable of dealing with several different problems in marine engineering, such as resistance, motion, sloshing, etc. (though not simulated here). Due to the discretization resolution, the method may be expensive for use in cases where the wavelength is very small as compared with the wave height. In that case one may consider a far-field approximation in

which vortex elements are lumped into equivalent vortices. As compared with the formulation based on the velocity potential, the current formulation can be regarded as a differential form (versus the integral form based on the velocity potential) of the dynamic equation on the free surface. This differential form offers certain advantages and disadvantages. It is easy to effect local treatments without affecting global results (e.g. in the treatment near an intersection of the body surface with the free surface), whereas the integral form of the equation tends to introduce cumulative effects near singular portions of the boundary of interest. The differential form of the equation obtains the field velocity directly instead of requiring an extra step of numerical differentiation. However, to get the pressure on the body, a numerical integration is required. One disadvantage is that the dynamic equation on the free surface is based on the slope of the free surface and not on the actual free surface elevation. Thus it is difficult to control the surface elevation as strictly governed by the gravitational restoring force; sometimes the mean water surface may be slightly off from the undisturbed position owing to accumulated numerical errors in a Lagrangian time-marching simulation.

The significance of the current work can be seen in the following aspects. First, it demonstrated the applicability and flexibility of vortex sheet modelling in the non-linear free surface flow problem. Secondly, it provides another non-linear analysis tool which may be useful in certain applications, e.g. in studying the loading on an offshore structure in large waves. Thirdly, it identified some advantages and disadvantages of an easy numerical approach to the study of wave–body and wave–wake interaction problems. It is hoped that numerical simulations using vortex method will find more and more applications in free surface problems of marine applications.

ACKNOWLEDGEMENTS

This work was sponsored by the United States Navy, Office of Naval Research, under Contract N000014-86-K-0058. Comments from Drs Robert Beck, Armin Troesch and Robert Krasny of The University of Michigan are deeply appreciated.

REFERENCES

1. T. Sarpkaya, 'Computational methods with vortices – the 1988 Freeman scholar lecture', *J. Fluids Eng.*, **111**, 5–52 (1989).
2. C. von Kerczek, 'Numerical solution of naval free surface hydrodynamics problems', in J. W. Schot and N. Salvesen (eds.), *Proc. Ist Int. Conf. on Numerical Ship Hydrodynamics*, Bethesda, MD, October 1975, pp. 11–47.
3. J. V. Wehausen and E. V. Laitone, 'Surface waves', in S. Flugge (ed.), *Encyclopedia of Physics, Vol. IX, Fluid Dynamics III*, Springer, Berlin, 1960.
4. B. Hunt, 'The mathematical basis and numerical principles of the boundary integral method for incompressible potential flow over 3-D aerodynamic configurations', in B. Hunt (ed.), *Numerical Methods in Applied Fluid Dynamics*, Academic, New York, 1980, pp 49–135.
5. M. S. Longuet-Higgins and E. D. Cokelet, 'The deformation of steep surface waves on water I. A numerical method of computation', *Proc. R. Soc. Lond. A*, **350**, 1–26 (1976).
6. M. Greenhow, T. Vinje, P. Brevig and J. Taylor, 'A theoretical and experimental study of the capsize of Salter's duck in extreme waves', *J. Fluid Mech.*, **118**, 221–239 (1982).
7. T. Vinje, M. Xie and P. Brevig, 'A numerical approach to nonlinear ship motion', *14th Symp. on Naval Hydrodynamics*, National Academy, New York, 1983, pp. 245–275.
8. S. J. Zaroodny and M. D. Greenberg, 'On a vortex sheet approach to the numerical calculation of water waves', *J. Comput. Phys.*, **11**, 440–446 (1973).
9. R. G. Zalosh, 'Discretized simulation of vortex sheet evolution with buoyancy and surface tension effects', *AIAA J.*, **14**, 1517–1523 (1976).
10. G. R. Baker, D. I. Meiron and S. A. Orszag, 'Generalized vortex methods for free surface flow problems', *J. Fluid Mech.*, **123**, 477–501 (1982).
11. J. G. Telste, 'Inviscid flow about a cylinder rising to a free surface', *J. Fluid Mech.*, **182**, 149–168 (1987).

12. J. C. S. Meng and J. A. L. Thomson, 'Numerical studies of some nonlinear hydrodynamic problems by discrete vortex element methods', *J. Fluid Mech.*, **84**, 433–453 (1978).
13. G. Tryggvason, 'Numerical simulations of the Rayleigh–Taylor instability', *J. Comput. Phys.* **75**, 253–282 (1988).
14. L. Chen, 'An application of vortex method to free surface flow problems', *Ph.D. Dissertation*, Department of Naval Architecture and Marine Engineering, University of Michigan, September 1990.
15. L. M. Milne-Thomson, *Theoretical Hydrodynamics*, MacMillan, London, 1968.
16. H. Lamb, *Hydrodynamics*, Cambridge University Press, Cambridge, 1932; Dover, New York, 1945.
17. G. R. Baker, D. I. Meiron and S. A. Orszag, 'Application of a generalized vortex method to nonlinear free-surface flows', in J.-C. Dern and H. J. Haussling (eds), *Proc. 3rd. Int. Conf. on Numerical Ship Hydrodynamics*, Paris, June 1981, pp. 179–191.
18. S. P. G. Dinavahi, 'A streakline method for computing vortical flows in two dimensions', *Ph.D. Dissertation*, Department of Naval Architecture and Marine Engineering, University of Michigan, 1988.
19. F. M. Deffenbaugh and F. J. Marshall, 'Time development of the flow about an impulsively started cylinder', *AIAA J.*, **14**, 908–913 (1976).
20. D. T. C. Porthouse and R. I. Lewis, 'Simulation of viscous diffusion for extension of the surface vorticity method to boundary layer and separated flows', *J. Mech. Eng. Sci.*, **23**, 157–167 (1981).
21. B. Maskew, 'A subvortex technique for the close approach to a discretized vortex sheet', *J. Aircraft*, **14**, 188–193 (1973).
22. T. H. Havelock, 'The wave resistance of a cylinder started from rest', *Q. J. Mech. Appl. Math.*, **2**, 325–334 (1949).
23. A. F. Teles da Silva and D. H. Peregrine, 'The nonlinear interaction between a free surface potential flow and a submerged cylinder', *Fourth Int. Workshop on Water Waves and Floating Bodies*, Oystese, May 1989, pp. 51–54.
24. N. Salvesen and C. H. von Kerczek, 'Numerical solutions of two-dimensional non-linear body–wave problems', *Proc. 1st Int. Conf. Numerical Ship Hydrodynamics*, Bethesda, MD, October 1975, pp. 279–293.